

# Quality control in the apoA-I secretory pathway: deletion of apoA-I helix 6 leads to the formation of cytosolic phospholipid inclusions

Shaila Bhat,<sup>1,\*</sup> Manal Zabalawi,<sup>1,\*</sup> Mark C. Willingham,<sup>\*</sup> Gregory S. Shelness,<sup>\*</sup> Michael J. Thomas,<sup>†</sup> and Mary G. Sorci-Thomas<sup>2,\*†</sup>

Departments of Pathology<sup>\*</sup> and Biochemistry,<sup>†</sup> Wake Forest University Health Sciences, Winston-Salem, NC

**Abstract** From a total of 47 known apolipoprotein A-I (apoA-I) mutations, only 18 are linked to low plasma HDL apoA-I concentrations, and 78% of these map to apoA-I helices 6 and 7 (residues 143–186). Gene transfer and transgenic mouse studies have shown that several helix 6 apoA-I mutations have reduced hepatic HDL production. Our objective was to examine the impact of helix 6 modifications on intracellular biosynthetic processing and secretion of apoA-I. Cells were transfected with wild-type or mutant apoA-I, radiolabeled with [<sup>35</sup>S]Met/Cys, and then placed in unlabeled medium for up to 4 h. Results show that >90% of newly synthesized wild-type apoA-I was secreted by 60 min. Over the same length of time, only 20% of helix 6 deletion mutant ( $\Delta 6$  apoA-I) was secreted, whereas 80% remained cell associated. Microscopic and biochemical studies revealed that cell-associated  $\Delta 6$  apoA-I was located predominantly within the cytoplasm as lipid-protein inclusions, whereas wild-type apoA-I was localized in the endoplasmic reticulum/Golgi. Results using other helix deletions or helix 6 substitution mutations indicated that only complete removal of helix 6 resulted in massive cytoplasmic accumulation. These data suggest that alterations in native apoA-I conformation can lead to aberrant trafficking and accumulation of apolipoprotein-phospholipid structures. Thus, conformation-dependent alterations in intracellular trafficking and turnover may underlie the reduced plasma HDL concentrations observed in individuals harboring deletion mutations within helix 6.—Bhat, S., M. Zabalawi, M. C. Willingham, G. S. Shelness, M. J. Thomas, and M. G. Sorci-Thomas. **Quality control in the apoA-I secretory pathway: deletion of apoA-I helix 6 leads to the formation of cytosolic phospholipid inclusions.** *J. Lipid Res.* 2004. 45: 1207–1220.

**Supplementary key words** apolipoprotein A-I • high density lipoprotein • mutant apolipoprotein A-I • protein secretion • quality control pathway • aggresomes • aggregation • endoplasmic reticulum • Golgi • nuclear envelope • immunofluorescence

Apolipoprotein A-I (apoA-I) is the major protein constituent of HDLs and is synthesized and secreted by the liver and intestine (1). This unique and abundant plasma protein directs mature spherical HDL particles to the liver, where the cholesteryl ester-rich core is removed by scavenger receptor class B type I, thereby completing a reverse cholesterol cycle (2–4). Completion of this cycle is thought to prevent the accumulation of cholesterol in the aorta and represents a mechanism explaining the high correlation between increased plasma HDL concentrations and a lower incidence of coronary heart disease in humans (5, 6).

Until recently, the origin of nascent HDL apoA-I in plasma was thought to occur by either direct secretion of “discoidal” structures from the liver, as shown by studies from perfused rat liver (7), or by rearrangement of intestinal remnants released from the lipolysis of triglyceride-rich lipoproteins or the association of phospholipids and apoA-I in plasma (8). Whereas VLDL particles have been readily isolated from the Golgi (9, 10), efforts to identify HDL particles along the secretory pathway have had little success (9). Although these findings provided little support for the intracellular assembly of nascent HDL, a number of other studies supported the concept of an intracellular apoA-I lipidation pathway (11–16). With the discovery of the ABCA1 transporter, many of these concepts concerning nascent HDL assembly have been revised, and recent studies support the idea of both ABCA1-dependent and -independent mechanisms responsible for apoA-I lipidation (17, 18).

The conformation of apoA-I is believed to be an essential factor regulating the synthesis, secretion, and lipidation of nascent HDL (19–22). Cataloging naturally occurring human apoA-I mutations associated with low HDL concentrations suggests that disruption of apoA-I’s native

Manuscript received 3 December 2003, in revised form 11 March 2004, re-revised form 25 March 2004, and in re-re-revised form 30 March 2004.

Published, JLR Papers in Press, April 1, 2004.  
DOI 10.1194/jlr.M300498-JLR200

<sup>1</sup> S. Bhat and M. Zabalawi contributed equally to this work.

<sup>2</sup> To whom correspondence should be addressed.  
e-mail: mstthomas@wfubmc.edu

structure dramatically alters HDL's intravascular metabolism (23). Of 18 documented apoA-I mutants associated with low HDL, 78% are amino acid substitutions/deletions within helices 6 and 7 (23). The association between mutant forms of helix 6 and 7 and aberrant HDL metabolism has been studied in mice by several different approaches. In one study, transgenic mice were created expressing  $\Delta 6$  apoA-I, a mutant form of apoA-I lacking the entire proline-punctuated 22 amino acid helix 6 (residues 143–164) (24, 25). In other studies, an adenoviral construct expressing the dominant-negative helix 6 point mutation, L159R apoA-I, was expressed in apoA-I knockout mice (26), and in yet another study, a targeted replacement for the dominant-negative mutant apoA-I Milano (R173C apoA-I), a helix 7 point mutation, was examined (27). In each of these studies, the data suggest that mutations within apoA-I helices 6 and/or 7 cause decreased hepatic production and contribute to the dominant-negative phenotype observed in individuals heterozygous for these mutations (23, 25).

Thus, the current studies were conducted to probe how apoA-I conformation affects intracellular trafficking and secretion by measuring the *in vitro* secretion efficiency of mutant forms of apoA-I compared with wild-type apoA-I. Combining biochemical and microscopy studies, we found that although wild-type apoA-I was localized mainly in the endoplasmic reticulum (ER)/Golgi compartment and was secreted efficiently, the helix 6 deletion mutation,  $\Delta 6$  apoA-I, was poorly secreted and accumulated within the cytosol as novel lipid-apolipoprotein structures. These studies show that deletion of a structurally essential helix results in the disruption of protein conformation and its accumulation and retention within the cell cytosol.

## MATERIALS AND METHODS

DMEM, DMEM/Coon's F12 (50:50), and G418 sulfate were obtained from Mediatech, Inc. Trypsin was obtained from JRH Biosciences, Inc. FuGene<sup>®</sup> was obtained from Roche Diagnostics Corp. Saponin was purchased from Sigma Chemicals. The polyclonal antibody to human apoA-I raised in goat was obtained from Chemicon, Inc. Rhodamine-conjugated antibody to goat IgG, mouse anti-cathepsin D, affinity-purified species-specific rabbit antiglobins conjugated with rhodamine or fluorescein, and BSA (IgG-free, protease-free) were purchased from Jackson ImmunoResearch Labs, Inc. Brefeldin A was obtained from Epicentre Technologies. Protein G-Sepharose 4 Fast Flow was purchased from Amersham Biosciences.

### Preparation of CMV5 human apoA-I cDNA-containing plasmids

Wild-type and all mutant forms of human apoA-I cDNA, as well as the human serum albumin cDNA, were cloned into the pCMV5 vector using previously established methods (28–30). PCR primers (CMV 5', 5'-GCCTGCAGTCCCCACGGCCCTT-3'; CMV 3', 5'-GCGGATCCCACTTTGGAAACG-3') containing embedded *Pst*I and *Bam*HI restriction sites, respectively, were used in the preparation of all clones. Introduction of apoA-I mutations was carried out as described previously (29–32). Constructs lacking the signal peptide sequence were made from human and

mutant forms of the human apoA-I cDNA using the 5' primer 5'-GCCTGCAGCGGCCCTTCAGGCGGCATTTCTGGCAG-3' and the same CMV 3' primer listed above. This 5' primer removes the entire 18 amino acid pre-apoA-I sequence, leaving the 6 amino acid "pro sequence" intact. All plasmids were grown and purified using the Maxi-prep kit (Promega) as previously described (28, 30).

### Cell culture maintenance and transfection

HepG2, COS-1, CHO-K1, and McArdle RH-7777 cells were obtained from the American Type Culture Collection. COS, HepG2, and McArdle RH-7777 cells were maintained in DMEM, whereas CHO cells were maintained in DMEM/Coon's F12 (50:50, v/v). All culture media contained essential vitamins and a final concentration of 100 U/ml penicillin, 100  $\mu$ g/ml streptomycin, 2 mM L-glutamine, and 10% FBS. Cells were maintained at 37°C in an atmosphere of 5% CO<sub>2</sub>.

Cells were routinely grown to near confluence (>95%) in T-75 flasks and then split every third day. The day before COS-1 cells were transfected, nearly confluent flasks were treated with trypsin (0.25% porcine trypsin, 0.02% EDTA) and seeded onto 35 mm dishes using a 1:60 dilution. Five to 6 h after seeding, cell monolayers at 25–30% confluence were transfected at a FuGene<sup>®</sup>-to-cDNA volume-to-mass ratio of 6:1 ( $\mu$ l/ $\mu$ g).

HepG2 cells were seeded onto 35 mm plates using a 1:40 dilution. Before plating, cells were passed through a 25 g syringe to prevent clumping. Approximately 24 h after plating, HepG2 cell monolayers reached 85% confluence and were transfected at a FuGene<sup>®</sup>-to-cDNA ratio of 2:1.25 ( $\mu$ l/ $\mu$ g). To reduce plate-to-plate transfection variability, duplicate plates of HepG2 cells per cDNA clone transfected were combined and replated 24 h after transfection.

CHO cells were stably transfected with the human apoA-I  $\Delta 6$  gene as previously described (29). These cells were routinely maintained in DMEM/Coon's F12 (50:50, v/v) containing a final concentration of 10% FBS, essential vitamins, 100 U/ml penicillin, 100  $\mu$ g/ml streptomycin, 2 mM L-glutamine, and 0.94 mg/ml G418.

Experiments involving brefeldin A were conducted on CHO  $\Delta 6$  apoA-I stably expressing cells that had been seeded onto 35 mm dishes at a 1:100 dilution from confluent T-75 flasks. Five to 6 h after plating, the cells were approximately 25–30% confluent. Cells were then treated with a final concentration of 2.5  $\mu$ M brefeldin A and then placed back into the incubator for 0, 24, and 48 h.

### Pulse-chase labeling and apoA-I immunoprecipitation

Forty-eight hours after transfection, metabolic labeling studies were performed. Cell monolayers were washed once with PBS (137 mM NaCl, 2.7 mM KCl, 8 mM Na<sub>2</sub>HPO<sub>4</sub>, and 1.46 mM KH<sub>2</sub>PO<sub>4</sub>, pH 7.4). Labeling was carried out by adding 0.5 ml of methionine-free DMEM (COS cells and HepG2 cells) or DMEM/Coon's F12 (50:50) (CHO cells) containing 10% fetal calf serum and 200  $\mu$ Ci/ml (18  $\mu$ l/35 mm dish) trans <sup>35</sup>S label or [<sup>35</sup>S]Met/Cys for 10 min as previously reported (33, 34). In some cases, metabolic labeling was continuous for up to 4 h or the indicated time. The chase was begun by aspirating the labeling medium and adding 0.5 ml of fresh methionine-free DMEM (COS cells and HepG2 cells) or DMEM/Coon's F12 (50:50) (CHO cells) containing 10% fetal calf serum only.

At the indicated times, the culture medium was removed and centrifuged to pellet cell debris. The medium was transferred to a new tube until immunoprecipitation. Cells monolayers were washed twice with PBS, scraped in 15 ml of PBS, and collected by centrifugation at 400 g for 5 min at 4°C. Unless otherwise indicated, all subsequent centrifugation steps were performed at 4°C. Cell pellets were suspended in 750  $\mu$ l of ice-cold lysis buffer

(25 mM Tris-HCl, pH 7.4, 300 mM NaCl, 1% Triton X-100, 1 mM PMSE, 10  $\mu$ g/ml leupeptin, and 10  $\mu$ g/ml pepstatin). After a 10 min incubation on ice, samples were centrifuged at 14,000 rpm for 2 min. The supernatants were transferred to a fresh microcentrifuge tube and adjusted to a final concentration of 2.5 mg/ml BSA. Cell pellets were immunoprecipitated by adding 30  $\mu$ l (2–3 mg/ml) of goat anti-human apoA-I antibody (Chemicon International, Inc.) and 35  $\mu$ l of Protein G-Sepharose beads suspended (50:50, v/v) in TBS-C (25 mM Tris-HCl, 140 mM NaCl, and 1 mM CaCl<sub>2</sub>). After incubating for 10–28 h at 4°C on a rotating wheel, immune complexes were recovered by centrifugation at 14,000 rpm for 30 s. Immune-complexed beads were washed twice with 1 ml of lysis buffer and once with 1 ml of TBS-C. Immunoprecipitation of conditioned culture medium was carried out exactly as with cell pellets except that 0.5 ml of medium was adjusted to 1 mg/ml BSA, then 30  $\mu$ l of goat anti-human apoA-I antibody and 35  $\mu$ l of Protein G-Sepharose were added. These pellets were washed a total of three times with TBS-C and then prepared for SDS-PAGE.

### SDS polyacrylamide gel electrophoresis, fluorography, and data quantification

ApoA-I eluted from the Protein G-Sepharose beads was separated by 15% SDS-PAGE as previously described (34). Gels containing <sup>35</sup>S-labeled proteins were dried and exposed to film at –80°C using Kodak Biomax MS film. Images were imported into Scion6 Image, and the signal areas were obtained from the gray scale image after calibrating the scanner as previously described (17).

### Preparation of postnuclear cell membranes

Transfected cells from 100 mm dishes were labeled as described above, their conditioned media were collected, and cells were then scraped from the dish using 1 ml of ice-cold hypotonic buffer (10 mM HEPES, pH 7.4, 1 mM PMSE, 10  $\mu$ g/ml leupeptin, and 10  $\mu$ g/ml pepstatin). The cells were recovered by centrifugation for 45 s at 14,000 rpm. After centrifugation, the supernatant was aspirated, and cell pellets were suspended in 1 ml of fresh hypotonic buffer and then incubated on ice for 15 min (33). The cell suspension was transferred to a 2 ml Dounce homogenizer and subjected to 20 strokes using a tight-fitting pestle. The homogenate was immediately adjusted to 250 mM (final concentration) sucrose and centrifuged at 3,000 rpm (700 g) for 10 min. The postnuclear supernatant was then transferred to a fresh microcentrifuge tube and subjected to an additional round of centrifugation as described above to ensure the complete removal of nuclei and unbroken cells. Pellets containing nuclei and unbroken cells were combined and saved for immunoprecipitation, whereas the supernatants from both spins were centrifuged at 200,000 g for 15 min using a TLA100.3 fixed-angle rotor to isolate the microsomal fraction. After this step, an aliquot of the supernatant or cell cytosolic fraction was saved for immunoprecipitation. The microsomal fraction or pellet from this spin was suspended using Dounce homogenization (tight pestle, 10 strokes) in 0.5 ml of 10 mM HEPES, pH 7.4, 250 mM sucrose, 10 mM NaCl, 10 mM KCl, 2.5 mM MgCl<sub>2</sub>, and 2.5 mM CaCl<sub>2</sub>, with the following final concentrations of protease inhibitors: 20  $\mu$ g/ml soybean trypsin inhibitor, 200  $\mu$ g/ml aprotinin, 2.5 mM PMSE, 25  $\mu$ g/ml leupeptin, and 25  $\mu$ g/ml pepstatin.

### Carbonate extraction of postnuclear cell membranes

The microsomal fraction was suspended in a final volume of 2 ml of ice-cold 0.1 M sodium carbonate, pH 11.5, using Dounce homogenization. The homogenized membranes were incubated on ice for 1 h and then centrifuged for 30 min at 200,000 g in a TL-100 tabletop ultracentrifuge. The microsomal pellet containing

noncarbonate-extractable proteins was saved for immunoprecipitation. The supernatant containing the carbonate-extractable microsomal proteins was also saved for immunoprecipitation. All fractions to be immunoprecipitated were adjusted to the following conditions: 50 mM Tris-HCl, pH 7.4, 200 mM NaCl, 70 mM Na<sub>2</sub>CO<sub>3</sub>, 1 mM CaCl<sub>2</sub>, and 1% Triton X-100. The final pH was adjusted to 7.4 by adding dilute HCl. Both supernatant and pellet fractions were adjusted to a final concentration of 1 mg/ml BSA, 1 mM PMSE, 10  $\mu$ g/ml leupeptin, and 10  $\mu$ g/ml pepstatin. The supernatant and pellet fractions were suspended in 800  $\mu$ l and 750  $\mu$ l of lysis buffer, respectively. Both suspensions were immunoprecipitated using 30  $\mu$ l of goat anti-human apoA-I polyclonal antibody and 70  $\mu$ l of Protein G-Sepharose according to the incubation conditions described above.

### Isolation of phospholipid:apoA-I complexes from postnuclear supernatant and slot-blot/Western analysis

To characterize cytoplasmic inclusion from the postnuclear supernatant, aliquots were adjusted to a density of 1.30 g/ml, overlaid with KBr solutions at 1.166, 1.066, and 1.006 g/ml, and then centrifuged using a SW-41 rotor for 44 h at 40,000 rpm at 15°C. The density of each fraction was obtained by weighing known volumes of the fractions recovered from blank gradients.

Phospholipid:apoA-I inclusions were isolated from HepG2 cell cytoplasmic extracts in hypotonic buffer after elution from an anti-human apoA-I affinity column as previously described (35). Both bound and unbound fractions were characterized for phospholipid and apoA-I content (36).

Slot-blot/Western analyses were carried out as previously described (24). Briefly, aliquots (100  $\mu$ l) from each fraction from the density gradient was applied to nitrocellulose (0.2  $\mu$ m) and then incubated with a polyclonal antibody to human apoA-I (1:2,000; Chemicon) and then to anti-goat IgG conjugated to alkaline phosphatase (1:4,000) and nitro blue tetrazolium/5-bromo-4-chloro-3-indolyl phosphate (Promega). The phospholipid content was determined on a pooled density fraction using established procedures (37).

### Data analysis

Images from X-ray film or nitrocellulose blots were scanned on a Linotype-Hell Ultra Scanner. Images were imported into Scion Image, and the densities were obtained from the gray scale image after calibrating the scanner as previously described (17).

### Immunofluorescence microscopy and morphometry

Cells were prepared for immunofluorescence microscopy as previously described (38–40). First, the monolayer was washed twice with PBS, and the cells were then treated with 1 ml of 3.7% formaldehyde in PBS for 10 min at room temperature. After fixing, the cells were washed three times with a solution of 1% BSA and 0.1% saponin prepared in PBS (BSA-saponin). The dishes were incubated for 10 min at room temperature to permeabilize the cell membrane and then were treated with a 1:2,500 dilution of anti-human apoA-I diluted in BSA-saponin for 30 min at room temperature. Cells were washed three times with PBS and incubated with a final concentration of 25  $\mu$ g/ml affinity-purified anti-goat IgG conjugated with rhodamine in BSA-saponin for 30 min. The cells were washed three times with PBS to remove unbound antibody and then fixed again with 1 ml of 3.7% formaldehyde for 10 min at room temperature.

For double-label experiments, cells were sequentially incubated in goat anti-apoA-I followed by mouse anti-cathepsin D (lysosomal marker). This step was followed by treatment with an affinity-purified species-specific rabbit antiglobin labeled with rhodamine. Lipid droplets were visualized by including the fluorescent lipid dye Nile Red or osmium-thiocarbohydrazide-



osmium that selectively labeled classic neutral lipid droplets (40). After postfixation, the cells were mounted using an anti-fade reagent, *p*-phenylenediamine, to retard photobleaching of the fluorescein signal. Before microscopy was performed, two drops of 90% glycerol was added in the center of the dish before mounting a cover slip. Microscopic analyses were carried using a Zeiss Axioplan-2 fluorescence microscope, and images were generated using a Dage MTI-300 charge coupled device camera. Visualization of images was performed using Adobe Photoshop.

Microscopic images were displayed in Adobe Photoshop, and the diameters of individual structures were measured in centimeters and converted to actual size (micrometers) based on the known magnification of the image. To obtain an average, ~10 diameters were used from six to eight different cells from duplicate plates.

## RESULTS

### Comparison of apoA-I secretion in hepatic and nonhepatic cells

The kinetics and efficiency of endogenous apoA-I secretion were examined in the human hepatoma cell line, HepG2. Because HepG2 cells normally synthesize and secrete apoA-I, plates of cells were mock transfected, pulsed for 10 min 48 h later with [<sup>35</sup>S]Met/Cys, and then chased for up to 4 h with medium containing an excess of amino acids. At the indicated time, apoA-I-containing cell lysates and medium were isolated, immunoprecipitated with anti-human apoA-I antibodies, and separated by SDS-PAGE followed by fluorography. Approximately 50% of the apoA-I made during the 10 min pulse was secreted into medium during the 30 min chase, as shown in **Fig. 1A**. After 60 min of chase, virtually all of the apoA-I formed during the pulse was secreted with the loss of cell pellet-associated apoA-I. Average results from multiple experiments are shown in **Fig. 1B** and suggest that by 30 min, 50% of the endogenous labeled apoA-I had been released by HepG2 cells, and that by 60 min, nearly 100% had been secreted. A similar kinetic profile was obtained from wild-type apoA-I-transfected HepG2 cells, differing only in the total amount of radiolabel secreted.

To explore whether the rapid and efficient secretion of apoA-I was unique to liver-derived cells, we examined apoA-I's secretory behavior in COS-1 cells, a nonhepatic, non-lipoprotein-producing cell line. COS-1 cells were transiently transfected with wild-type human apoA-I and then metabolically labeled as described above for HepG2 cells. The results shown in **Fig. 1C, D**, left panels, indicate that by ~240 min only 35–40% of the newly synthesized apoA-I was secreted into the medium, whereas ~60% remained associated with the cell pellet. These results demonstrate a sluggish and less efficient secretion of apoA-I from COS-1 cells compared with HepG2 cells. Less efficient secretion of apoA-I from COS-1 cells does not appear to be related to overexpression, because COS-1 cells transiently transfected with a cDNA encoding human serum albumin showed similar initial counts of radiolabeled protein, with a secretion profile similar to that of apoA-I by HepG2 cells. However, unlike HepG2 cells, COS-1 cells consistently showed an additional higher molecular weight

band that likely represents the “pro” apoA-I form of mature human apoA-I (14, 41, 42). However, the ratio of bands in the apoA-I doublet did not appear to vary during the pulse-chase analysis, suggesting that the pro form can be processed and secreted at a similar rate as the mature form. We have also explored the possibility that the association of newly secreted apolipoprotein with the plasma membrane could explain the apparent low secretion efficiency in COS-1 cells. However, pretreatment of transfected pulsed-labeled COS-1 cells with trypsin before immunoprecipitation of the cell pellet did not alter the results (our unpublished observations).

### ApoA-I conformation affects secretion kinetics regardless of cell type

ApoA-I helix 6, one of seven proline-punctuated 22 amino acid helices in apoA-I, plays an essential role in determining its lipid-bound conformation (19, 23, 26, 29, 31, 32). Transgenic mice expressing a helix 6 deletion mutant ( $\Delta 6$  apoA-I) have remarkably low concentrations of mature HDL. A reduced rate of apoA-I HDL production has been cited as a contributing factor to the low circulating levels of HDL in Tg  $\Delta 6$  apoA-I mice (24). To understand the basis of the low hepatic production of  $\Delta 6$  apoA-I, we examined its secretory behavior in HepG2 cells. HepG2 cells were transfected with a cDNA encoding human  $\Delta 6$  apoA-I, and the time course of apoA-I secretion was recorded. Quantitative analysis of both exogenous transfected mutant  $\Delta 6$  apoA-I (**Fig. 2B**) and endogenous wild-type apoA-I (**Fig. 2C**) was possible because of differences in molecular size and migration during SDS-PAGE, shown in **Fig. 2A**. Pulse-chase analyses demonstrated that  $\Delta 6$  apoA-I was poorly secreted from HepG2 cells, with less than 25% of the initial radiolabel secreted by 240 min and more than 70% of the radiolabel remaining cell associated. In contrast, the endogenous wild-type apoA-I in the transfected HepG2 cells was secreted with a half-life of ~45 min and an efficiency of ~100%, similar to the results for mock-transfected cells in **Fig. 1**.

To examine the structural impact of deleting helix  $\Delta 6$ , the secretion kinetics of other apoA-I mutants were also examined, as shown in **Fig. 3**. COS-1 cells were transfected, and 48 h later the medium and cell pellets were analyzed as before. These data suggest that substitution of helix 6 with helix 10, 10F6 apoA-I (31), had little effect on its secretion kinetics (**Fig. 3A**) when compared with wild-type apoA-I. On the other hand, two point mutations that functionally disrupt helix 6 either by introducing a charged amino acid into its hydrophobic face (L159R apoA-I) (23, 43, 44) or by introducing a proline at the center of its amphipathic  $\alpha$ -helix showed significantly reduced secretion efficiency. Additionally, deletion of individual 22-mers had little effect on secretion except in the case of either helix 6 or helix 7 (**Fig. 3B**). Deletion of helix pairs or 44-mers (**Fig. 3C**) also had relatively little effect on secretion, including the deletion of the helix pairs 5/6 and 7/8. Overall, the data in **Fig. 3** suggest that conformational alterations induced by the deletion of single helices 6 and 7 had greater structural impact on apoA-I folding and secre-



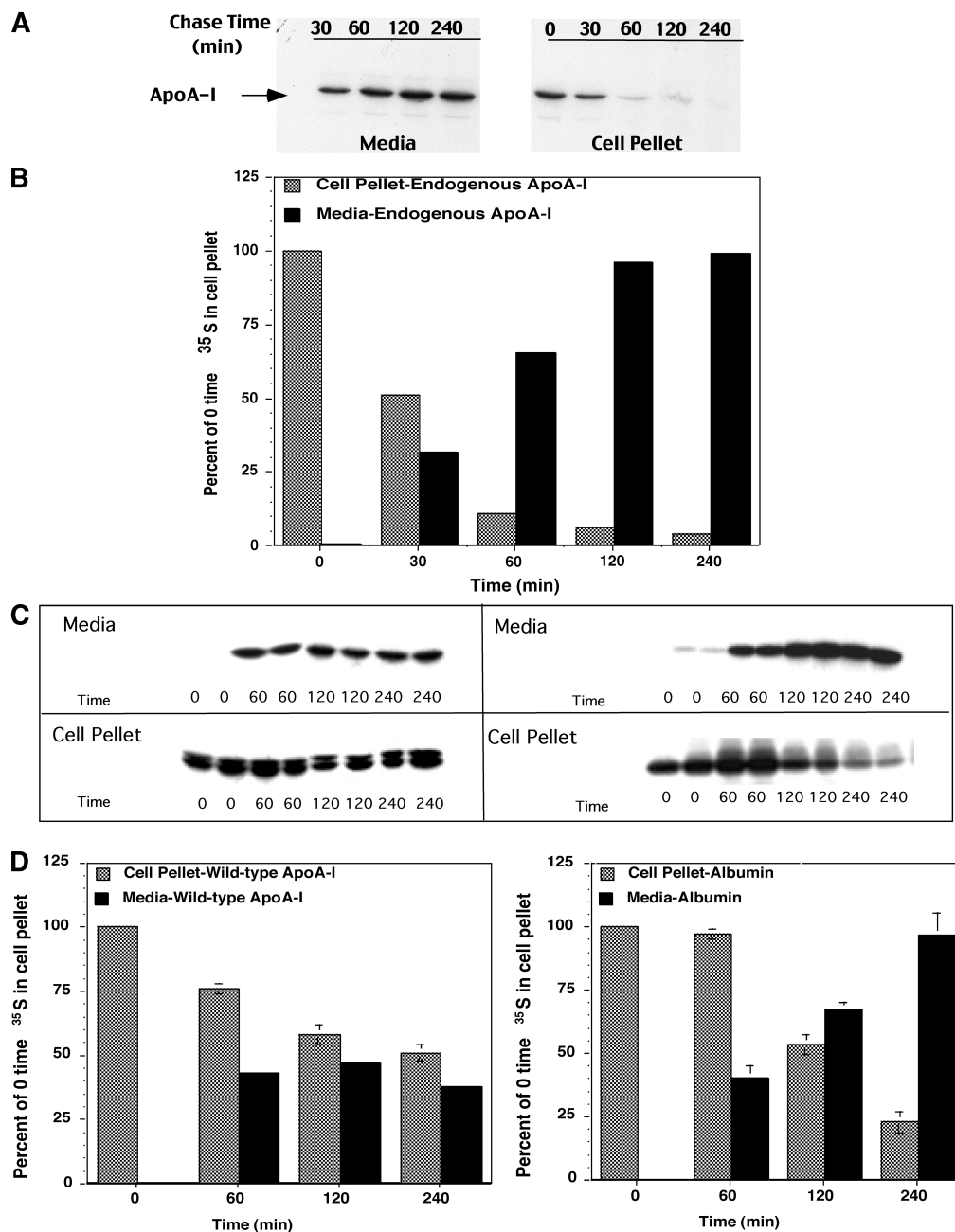


**Fig. 1.** Time-course secretion of apolipoprotein A-I (apoA-I) from HepG2 and COS-1 cells. Subconfluent dishes of either HepG2 cells (A and B) or transiently transfected COS-1 cells (C and D) were studied to compare the rates of newly synthesized apoA-I secretion. HepG2 cells were mock transfected and COS-1 cells were transiently transfected with human apoA-I cDNA under the control of the CMV5 promoter, as described in Materials and Methods. Twenty-four hours after transfection, cells were pulsed for 10 min with [<sup>35</sup>S]Met/Cys and then chased for various times up to 4 h. Both media and cell pellets were immunoprecipitated with a polyclonal antibody to human apoA-I run on 15% SDS-PAGE and imaged by fluorography. A: Secretion and accumulation of newly synthesized apoA-I from HepG2 cells with time and the reciprocal decrease in cell lysate apoA-I with time. B: Quantification of radioactivity data from HepG2 cell medium (black bars) and cell lysate (gray bars), where the y axis is expressed as a percentage of 0 time <sup>35</sup>S in the cell pellet. C: Time-course secretion of human apoA-I (left) and human serum albumin (right) from transfected COS-1. COS-1 cells were transiently transfected with either human apoA-I cDNA or human serum albumin cDNA under the control of the CMV5 promoter, as described in Materials and Methods. Twenty-four hours after transfection, duplicate dishes were trypsinized and replated for each clone indicated. Forty-eight hours after transfection, cells were pulsed for 10 min with [<sup>35</sup>S]Met/Cys. After the pulse, culture medium was replaced with unlabeled medium and the cells were incubated for the indicated time. Cell detergent lysates and media samples were subjected to immunoprecipitation with a polyclonal antibody to human apoA-I, as described in Materials and Methods. D: Quantification of radioactivity data from COS-1 cell medium (black bars) and cell lysate (gray bars), where the y axis is expressed as a percentage of 0 time <sup>35</sup>S in the cell pellet. Error bars represent the SD of at least three independent experiments.

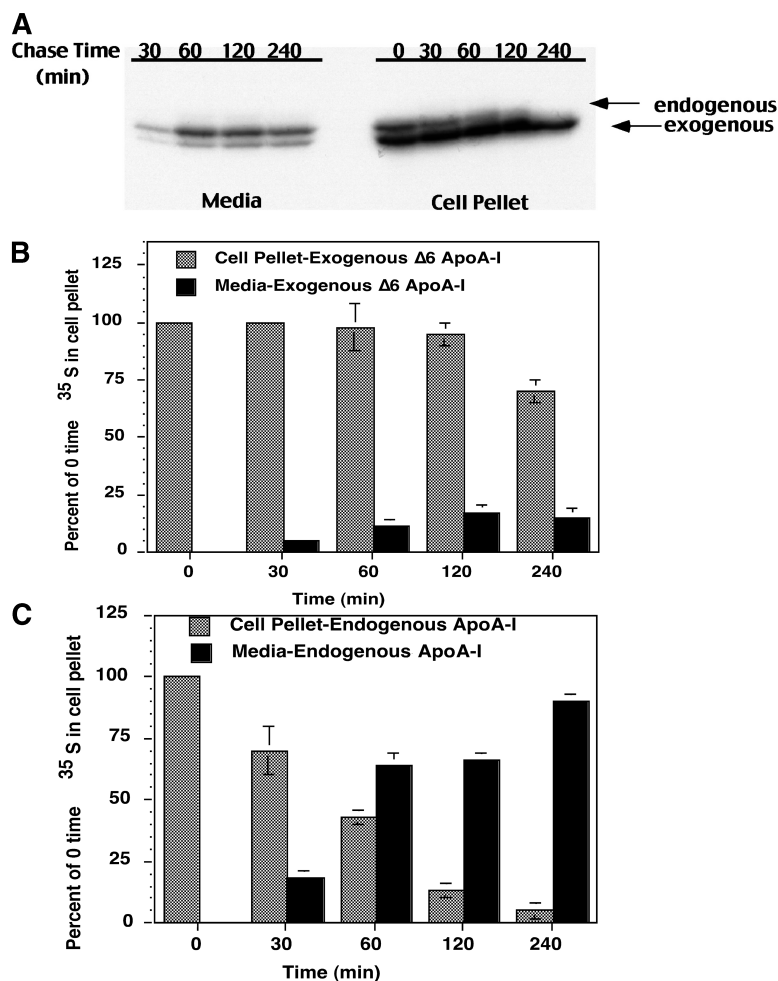


**Fig. 2.** Time-course secretion of wild-type and  $\Delta 6$  apoA-I from HepG2 cells. Subconfluent dishes of HepG2 cells were transiently transfected with human  $\Delta 6$  apoA-I cDNA under the control of the CMV5 promoter, as described in Materials and Methods. Twenty-four hours after transfection, cells were pulsed for 10 min with [ $^{35}\text{S}$ ]Met/Cys and then chased for various times up to 4 h. Both media and cell pellets were immunoprecipitated with a polyclonal antibody to human apoA-I run on 15% SDS-PAGE and imaged by fluorography. A: Results of cell detergent lysates and media samples that were subjected to immunoprecipitation with a polyclonal antibody to human apoA-I and then analyzed by 15% SDS-PAGE and fluorography. B: Quantification of newly synthesized exogenous apoA-I from HepG2 cell medium (black bars) and cell pellet lysate (gray bars). C: Quantification of endogenous apoA-I in culture medium (black bars) and associated with the cell pellet (gray bars). In HepG2 cells, the  $^{35}\text{S}$  labeling of endogenous (wild-type) apoA-I could be separated from the labeled exogenous apoA-I, corresponding to transfected  $\Delta 6$  apoA-I (missing 22 residues) by virtue of the difference in molecular size on 15% SDS-PAGE. Error bars represent the SD of at least three independent experiments.

tion than did the deletion of helix pairs. COS-1 cells were used in these experiments because they lack any complication attributable to endogenous wild-type apoA-I production. Parallel experiments were conducted using HepG2 cells with similar results.

#### Immunofluorescence pattern of wild-type and $\Delta 6$ apoA-I in cells

The strikingly inefficient secretion of  $\Delta 6$  apoA-I from HepG2 cells was also demonstrated in non-lipoprotein-producing cell lines (i.e., CHO and COS-1). These observations prompted an investigation to determine the location of the retained  $\Delta 6$  apoA-I within the cell. Both COS-1 and HepG2 cells were either mock transfected or transfected with wild-type or  $\Delta 6$  apoA-I cDNA. **Figure 4A** shows the immunofluorescence detection pattern for mock-transfected HepG2 cells, and Fig. 4B, C shows wild-type apoA-I and  $\Delta 6$  apoA-I, respectively, in transfected COS-1 cells. The discernible nuclear envelope-ER and Golgi pattern observed in Fig. 4A is typical of a conventional secretory protein. The fluorescence distribution in mock-transfected HepG2 cells appears identical to COS-1 cells transfected with wild-type apoA-I (Fig. 4B). COS-1 cells appear brighter as a result of the transfected exogenous apoA-I and the fact that they have virtually no detectable

endogenous apoA-I signal by immunofluorescence. It is likely that transfected COS-1 cells appear brighter in part because of the slower and less efficient secretion kinetics relative to HepG2 cells. Thus, in a transfected, non-lipoprotein-producing cell line such as COS-1, the nuclear envelope-ER/Golgi fluorescence pattern was similar to the endogenous wild-type apoA-I distribution in HepG2 cells.

In contrast to the typical ER/Golgi staining pattern,  $\Delta 6$  apoA-I-transfected COS-1 cells showed the formation of cytoplasmic inclusions and very little ER/Golgi staining. The distribution of fluorescent  $\Delta 6$  apoA-I, combined with the pulse-chase data shown in Fig. 2, suggests that very little of the  $\Delta 6$  apoA-I protein travels through the classic secretory pathway but may be shunted into a cytosolic quality control pathway as a consequence of the mutant proteins' altered conformation. The fluorescent structures in  $\Delta 6$  apoA-I-expressing cells appear circular in shape, with a diameter of 1.4  $\mu\text{m}$ , and show bright perimeter labeling. We call these apoA-I cytoplasmic structures "bagels." These structures were consistently observed in HepG2 and CHO cells transiently or stably transfected with  $\Delta 6$  apoA-I cDNA. Stably transfected CHO cells expressing  $\Delta 6$  or wild-type apoA-I showed apoA-I fluorescent staining patterns identical to those seen with transiently transfected COS-1 cells (data not shown). When  $\Delta 6$  apoA-

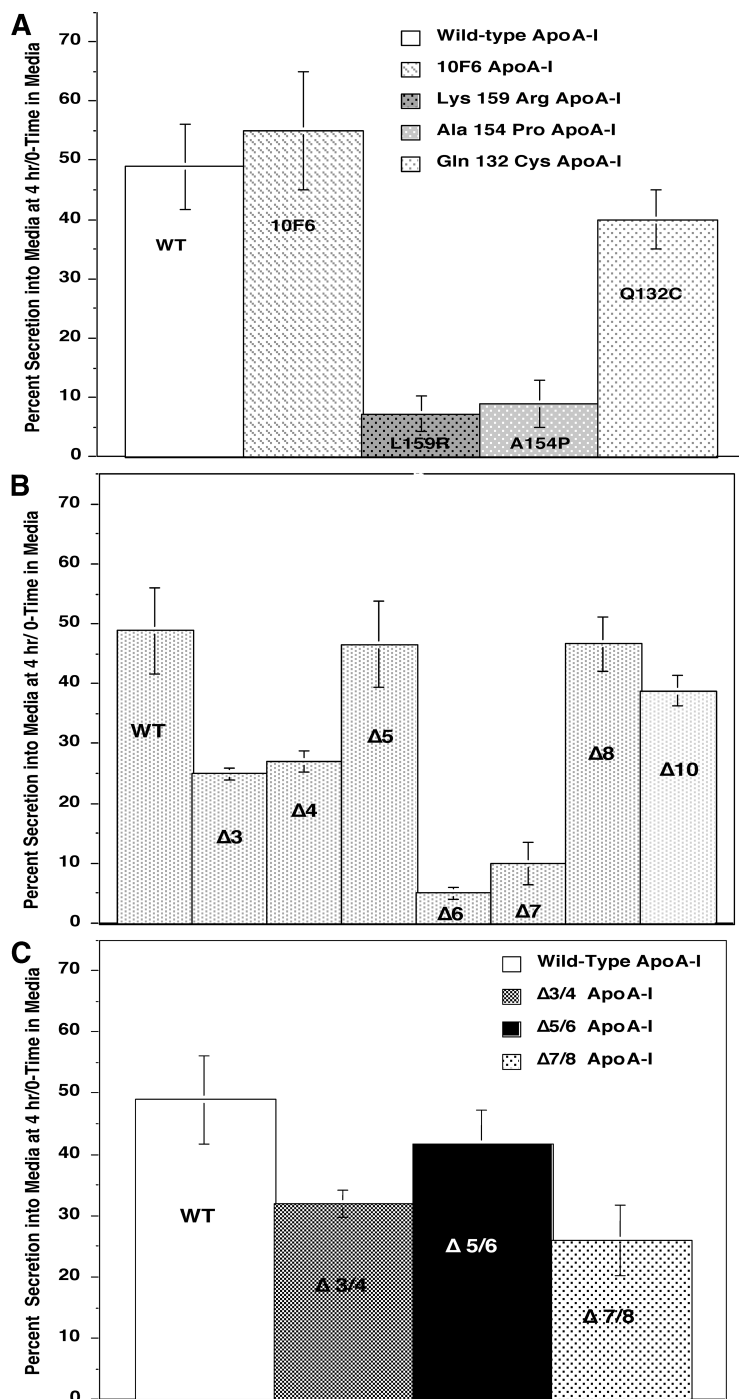


**Fig. 3.** Secretion of wild-type (WT) and mutant apoA-I from COS-1 cells. Subconfluent dishes of COS-1 cells were transiently transfected with human wild-type or mutant apoA-I cDNA under the control of the CMV5 promoter, as described in Materials and Methods. Twenty-four hours after transfection, cells were pulsed for 10 min with [<sup>35</sup>S]Met/Cys and then chased for various times up to 4 h. Both media and cell pellets were immunoprecipitated with a polyclonal antibody to human apoA-I run on 15% SDS-PAGE and imaged by fluorography. The y axis is expressed as the amount of radioactivity secreted into the media divided by the 0 time <sup>35</sup>S in the cell pellet × 100. A: Relative secretion efficiency for apoA-I replacement mutants: 10F6 apoA-I, a mutant in which helix 10 has been placed in the position of helix 6 (31); L159R apoA-I, the human dominant-negative mutant termed apoA-I Fin (43, 44), in which a positively charged residue has been placed in the center of the hydrophobic face of helix 6; A154P apoA-I, in which a proline residue replaces an alanine on the hydrophilic face of helix 6; and Q132C apoA-I (30), a mutant that allows disulfide formation between monomers of apoA-I within helix 5. B: Relative secretion efficiency for apoA-I deletion mutations for entire 11-mer and 22-mer domains: Δ3, deletion of residues 88–98; Δ4, deletion of residues 99–120; Δ5, deletion of residues 121–142; Δ6, deletion of residues 143–164; Δ7, deletion of residues 165–186; Δ8, deletion of residues 187–208; Δ10, deletion of residues 220–241. C: Relative secretion efficiency for apoA-I deletion mutations for entire 44-mers (32). Error bars represent the SD of at least three independent experiments.

I-expressing CHO cells were incubated with 2.5 μM brefeldin A, the cytoplasmic inclusions decreased in number but increased in diameter to ~2 μm by 48 h and to 5 μm by 72 h (data not shown), suggesting the fusion of preformed inclusions.

#### Subcellular localization of retained mutant apoA-I

To verify the cytoplasmic location of the retained Δ6 apoA-I, we performed subcellular fractionation studies as described in Materials and Methods. HepG2 cells were transiently transfected with either Δ6 or wild-type apoA-I. Forty-eight hours after transfection, cells were continu-

ously labeled for 3 h with [<sup>35</sup>S]Met/Cys. Postnuclear, cytosolic, and microsomal fractions were obtained as described previously, subjected to immunoprecipitation with anti-apoA-I antibodies, and then run on SDS-PAGE, as shown in **Fig. 5A**. Quantification of these data in **Fig. 5B** reveals that although ~20–30% of the total labeled wild-type apoA-I accumulated in the cytosolic fraction (lane 2), ~70–80% of the Δ6 apoA-I accumulated in this same fraction (lane 6). The ER-extractable fractions showed similar amounts of lipidated (lanes 3 and 7) and nonlipidated (lanes 4 and 8) apoA-I for both wild-type and Δ6 apoA-I-transfected HepG2 cells. Thus, these results suggest that



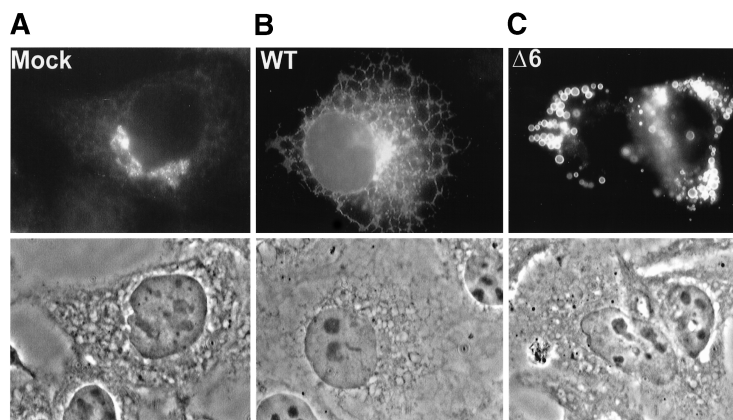


**Fig. 4.** Immunofluorescence staining of apoA-I in transfected HepG2 and COS-1 cells. These photomicrographs show the immunofluorescence staining of cells that had been fixed with formaldehyde 48 h after transfection and then processed using a polyclonal antibody to human apoA-I and rhodamine indirect labeling, as described in Materials and Methods. Directly below each micrograph is its corresponding phase-contrast image. A: Mock-transfected HepG2 cells show the endogenous apoA-I staining characterized by a weak endoplasmic reticulum (ER)/Golgi pattern. B: Transfection of COS-1 cells with wild-type (WT) apoA-I. HepG2 cells show very similar results only brighter, because the staining in these cells includes both the endogenous and exogenous signals. ApoA-I secretion is characterized by the presence of a bright nuclear envelope-ER/Golgi pattern. C: COS-1 cells transfected with  $\Delta 6$  apoA-I. In these studies, the cell shows circular cytoplasmic droplets labeled brightly at their edges, termed “bagels.” Note that both transfected CHO and McArdle RH-7777 cells show structurally similar inclusions (bagels) when transfected with  $\Delta 6$  apoA-I (data not shown).

the difference in accumulation between wild-type and  $\Delta 6$  apoA-I-expressing cells does not result from differences in lipidation within the ER lumen. Mock-transfected cells showed levels of radiolabeled endogenous apoA-I  $\sim 50$ -fold lower than those in wild-type apoA-I transfected cells, indicating that the endogenous apoA-I background expression did not interfere with data interpretation.

#### Cytosolic intracellular $\Delta 6$ apoA-I associates with phospholipid

To determine the extent of intracellular  $\Delta 6$  apoA-I lipidation, the postnuclear supernatant was isolated, adjusted to a density of 1.30 g/ml, and subjected to density gradient ultracentrifugation. As shown in **Fig. 6A**, 24 fractions were taken from each centrifuge tube and the density of each fraction was determined from its refractive index. An aliquot from each fraction was removed and assayed for apoA-I and apoB content by slot-blot/Western analysis. HepG2 cells transfected with  $\Delta 6$  apoA-I showed a large amount of buoyant or lipid-associated material that contained protein that bound anti-human apoA-I antibodies. Both  $\Delta 6$  and wild-type apoA-I-transfected HepG2 cells contained low but similar amounts of buoyant apoB-containing material, but these levels were significantly lower than the  $\Delta 6$  apoA-I content in the cytosolic fraction from transfected HepG2 cells. Individual fractions were pooled according to their density, dialyzed, and then assayed for phospholipid and triglyceride content. Figure 6B shows that the phospholipid content of the 1.056–1.160 g/ml density fraction from  $\Delta 6$  apoA-I-transfected cells had a 6-fold higher mass of phospholipid than cells transfected with wild-type apoA-I. Neither triglyceride nor cholesterol was found in any of the fractions (data not shown).

The lipid-to-protein composition of the cytoplasmic complexes was examined in more detail after their isolation using anti-apoA-I affinity chromatography. HepG2 cells were transfected with either wild-type or  $\Delta 6$  apoA-I cDNA, and 48 h later the postmicrosomal supernatant or cytosolic fraction was prepared and applied to an anti-human apoA-I affinity column. The column was washed extensively to remove unbound material, and then the apoA-I-containing material was eluted using a sodium isothiocyanate elution buffer. The bound fraction was extensively dialyzed, and its phospholipid and apoA-I composition was determined. Wild-type apoA-I-transfected cells contained little apoA-I. The small amount of material recovered from wild-type transfected cells had  $\sim 5$  mol of phospholipid to 1 apoA-I. In contrast, the cytosolic fraction from  $\Delta 6$  apoA-I-transfected HepG2 cells had a much larger amount of apoA-I eluting from the affinity column, with  $\sim 35$ – $40$  molecules of phospholipid to 1 mutant apoA-I (two independent experiments). Unbound fractions were also analyzed and found to contain 600–750 molecules of phospholipid to apoA-I and were similar among all cytosolic fractions analyzed.

#### Do $\Delta 6$ apoA-I and phospholipid inclusions represent aggresomes?

During protein synthesis, misfolded proteins are either retained within the ER and degraded immediately or exported from the ER to the cytosol, where they are incorporated into proteasomes and degraded. When the amount of exported misfolded protein exceeds the capacity of the proteasome, the accumulated proteins form complexes or structures termed “aggresomes” that tend to collect around the centrosome (45, 46). However, the formation of aggre-

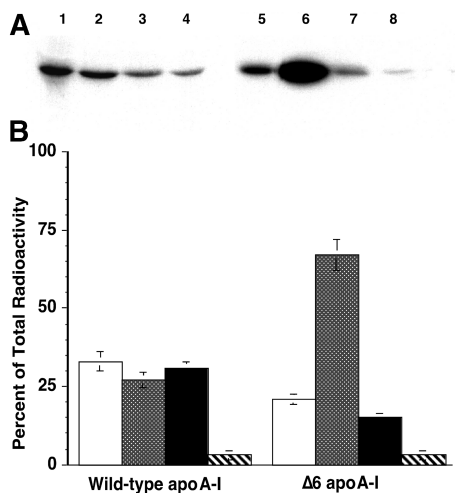


**Fig. 5.** Subcellular fractionation of apoA-I from transfected HepG2 cells. **A:** HepG2 cells were transiently transfected with human wild-type (lanes 1–4) or  $\Delta 6$  apoA-I (lanes 5–8) cDNA. Twenty-four hours later, duplicate transfection dishes were trypsinized and replated for each clone. Forty-eight hours after transfection, cells were continuously labeled for 3 h with [ $^{35}$ S]Met/Cys, after which cells were washed, suspended in hypotonic buffer, and processed as described in Materials and Methods. Postnuclear pellets were combined and saved for immunoprecipitation (lanes 1 and 5). The postnuclear supernatant was centrifuged at 200,000  $g$  for 15 min using a TLA100.3 fixed-angle rotor. From this spin, the supernatant was saved for immunoprecipitation and represents the transfected cell cytosol (lanes 2 and 6). Pellets from the postnuclear membrane isolation were suspended by Dounce homogenization, and the microsomes were adjusted to 0.1 M sodium carbonate, pH 11.5, and incubated on ice for 1 h. The membranes were then centrifuged for 30 min at 200,000  $g$  in a TL-100 tabletop ultracentrifuge, and the microsome pellet containing noncarbonate-extractable proteins was saved for immunoprecipitation (levels below detection limit; data not shown). The supernatant fraction or carbonate-extractable microsomal proteins were adjusted to  $d = 1.25$  g/ml with KBr and ultracentrifuged to determine the amount of lipidated ( $d < 1.25$  g/ml; lanes 3 and 7) or nonlipidated ( $d > 1.25$  g/ml; lanes 4 and 8) apoA-I after immunoprecipitation. Immunoprecipitation of each of these fractions was carried out, and the fraction was run on 15% SDS-PAGE and analyzed by fluorography. **B:** Quantification of immunoreactive radiolabeled apoA-I (expressed as the percentage of total radioactivity) for wild-type and  $\Delta 6$  apoA-I-expressing HepG2 cells. Mock-transfected cells showed levels of endogenous apoA-I radiolabel incorporation  $\sim 50$ -fold lower than that for transfected cells. Error bars represent the SD of at least three different experiments.

some-like structures may occur by alternative pathways. For example, ER-exported amyloid  $\beta$ -peptide has been reported to escape degradation by the proteasome, yet it was not incorporated into “classic” cytosolic aggresomes (47), suggesting that distinct aggregation pathways may exist for proteins exported from the ER to the cytosol, rather than only one major pathway. Therefore, it is possible that the formation of cytosolic inclusions or structures may result not only from increased generation of an aggregating protein but also from the reduced clearance or degradation of misfolded protein (48).

To assess the extent to which intracellular  $\Delta 6$  apoA-I inclusions resemble aggresomes, immunofluorescence stud-

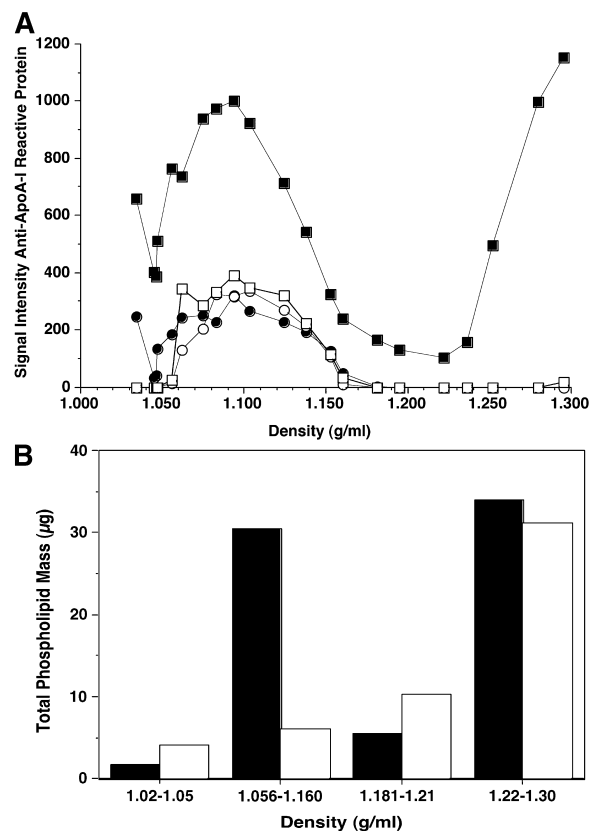


**Fig. 6.** Gradient ultracentrifugation of postnuclear supernatant from HepG2 cells transfected with  $\Delta 6$  apoA-I. HepG2 cells were transfected with either wild-type or  $\Delta 6$  apoA-I cDNA, and 48 h later cell monolayers were washed and lysed using the same conditions as outlined in Materials and Methods. **A:** The postnuclear supernatant was centrifuged, and the cell cytosol was adjusted to a density of 1.30 g/ml with KBr overlaid with KBr solutions of density 1.166, 1.066, and 1.006 g/ml and then spun at 40,000 rpm for 48 h in a SW41 rotor. After centrifugation, the contents were fractionated and their densities determined. Slot-blot/Western analyses were performed on individual fractions, and total apoA-I (squares) and apoB mass (circles) were determined using specific polyclonal antibodies, as described in Materials and Methods. Closed squares and circles represent the apoA-I and apoB mass from  $\Delta 6$  apoA-I-transfected cells, and open squares and circles represent the apoA-I and apoB from wild-type apoA-I-transfected HepG2 cells. ApoA-I levels were lowest in wild-type transfected cells, whereas apoB levels in both  $\Delta 6$  and wild-type transfected cells were similarly low. Although traces of apoA-I and apoB were found in cell lysates of transfected HepG2 cells, it appeared that  $\Delta 6$  apoA-I-transfected cells accumulated large amounts of  $\Delta 6$  apoA-I. **B:** The mass of phospholipid associated with each of the indicated density ranges for wild-type transfected cells (open bars) and  $\Delta 6$  apoA-I-transfected cells (closed bars). The cell cytosol from  $\Delta 6$  apoA-I-transfected HepG2 cells accumulated 6-fold more protein-associated phospholipid floating at a density of 1.056–1.160 g/ml compared with wild-type apoA-I-transfected HepG2 cells.

ies were conducted in COS-1 cells expressing low and high levels of wild-type and mutant forms of apoA-I. Two mutant forms of apoA-I were chosen that had been shown to secrete less than 10% of their initial radioactivity into the culture medium after 4 h of chase (Fig. 3) compared with COS-1 cells transfected with wild-type apoA-I, which secrete  $\sim 40$ –50% of their radioactivity after 4 h (Fig.

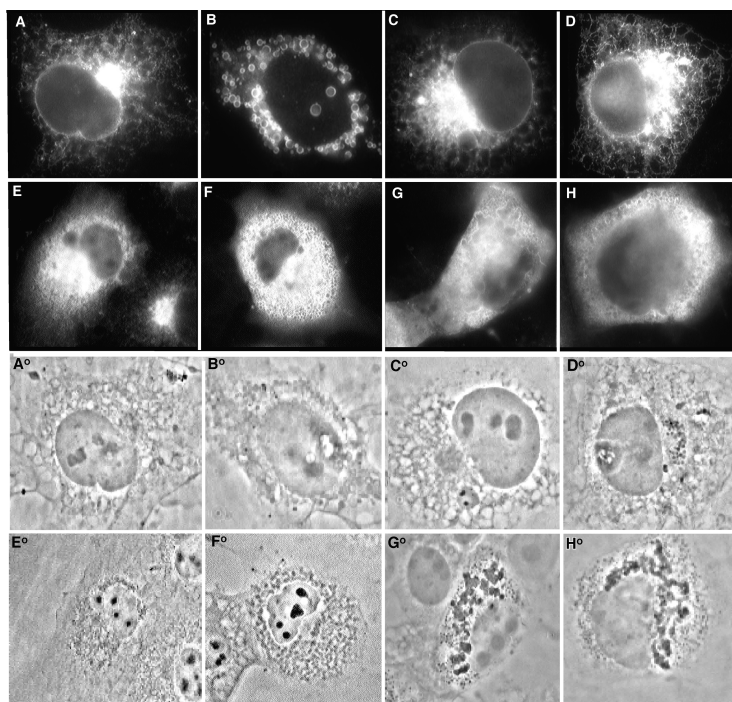


**Fig. 7.** Immunofluorescence of COS-1 cells transfected with wild-type and mutant forms of apoA-I. COS-1 cells were transfected with wild-type and mutant forms of apoA-I, and 48 h later the cells were permeabilized and processed as described in Materials and Methods. A–D: Immunofluorescence images from low-apoA-I-expressing COS-1 cells; A°–D°: the corresponding phase-contrast images. E–H: Immunofluorescence images from high-apoA-I-expressing cells; E°–H°: the corresponding phase-contrast images. A and E show cells transfected with wild-type apoA-I; B and F show cells transfected with  $\Delta 6$  apoA-I; C and G show cells transfected with L159R apoA-I, a point mutation associated with a dominant-negative phenotype in humans carrying the heterozygous form of this apoA-I mutation; and D and H show cells transfected with A154P apoA-I, a point mutation that interrupts the helix 6 (amino acids 143–164) 22-mer by the substitution of a proline, breaking the 22-mer into two 11-mers and essentially removing its lipid binding properties.

1). The immunofluorescence pattern and corresponding phase-contrast images of low-apoA-I-expressing cells are shown in **Fig. 7A–D** and A°–D°, respectively. Fig. 7E, F and E°, F° show the immunofluorescence and phase-contrast images of high-apoA-I-expressing COS-1 cells, respectively.

In cells expressing low levels of wild-type apoA-I, immunofluorescence was confined to the nuclear envelope, ER, Golgi, and plasma membrane (Fig. 7A). In cells expressing high levels of wild-type apoA-I, a saturation point was reached at which protein aggregation occurred, typified by the presence of dense, irregularly shaped inclusions readily seen by phase-contrast microscopy. These structures represent misfolded and/or aggregated apolipoproteins that have apparently overwhelmed the quality control pathway (Fig. 7E, E°). On the other hand, cells expressing low levels of  $\Delta 6$  apoA-I displayed large, uniformly shaped cytoplasmic inclusions (bagels in Fig. 7B) and contained few, if any, phase-dense structures (Fig. 7B°). Cells expressing high levels of  $\Delta 6$  apoA-I (Fig. 7F, F°) produced more phase-dense structures with an overall appearance that was similar to the pattern of phase-dense material observed in cells overexpressing wild-type apoA-I.

Additional experiments were conducted to examine the immunofluorescence pattern for other forms of apoA-I that have mutations in the helix 6 domain. The helix 6 point mutant, L159R apoA-I (i.e., apoA-I Fin), was chosen because we (Fig. 3) and others (26) have found it to have poor secretion efficiency. However, despite the aberrant secretion efficiency, as measured by pulse-chase studies, both the immunofluorescence and phase-contrast patterns for low- and high-expressing COS-1 cells (Fig. 7C, G and C°, G°) appeared to be similar to the immunofluorescence patterns observed for COS-1 cells transfected with wild-type apoA-I, respectively.

Another helix 6 apoA-I mutant, A154P apoA-I, effectively removes a lipid binding domain by virtue of a proline-for-alanine substitution in the middle of the amphipathic helix, breaking the 22 residue domain in half. This mutation induces similar secondary structural alterations as those observed for  $\Delta 6$  apoA-I and renders a low (<10%) secretion efficiency, as determined by pulse-chase studies (Fig. 3). The immunofluorescence and phase-contrast patterns are shown in Fig. 7D, D°. Cells expressing low levels of A154P apoA-I showed a ER/Golgi staining pattern, whereas cells expressing high levels of A154P apoA-I contained mostly dense, irregular shaped aggresomes (Fig. 7H, H°). It appears that low-expressing  $\Delta 6$  apoA-I COS-1 cells contained round, uniformly sized cytoplasmic inclusions (Fig. 7B), whereas COS-1 cells expressing high levels of apoA-I were typified by intensely fluorescent cytoplasmic inclusions with highly dense, irregular shapes. These observations suggest that the unique structures found in low-expressing  $\Delta 6$  apoA-I cells are not the product of protein overexpression.

#### Accumulation and degradation of cytosolic $\Delta 6$ apoA-I inclusions

Misfolded  $\Delta 6$  apoA-I may be either prevented from entering the ER during synthesis or expelled from the ER shortly thereafter, when the misfolded apolipoprotein enters the quality control pathway (49). To distinguish between these possibilities, constructs were created that express wild-type and  $\Delta 6$  apoA-I cDNAs lacking their signal peptide sequence, which would prevent the apolipoproteins from entering the ER lumen. We hypothesized that both wild-type and  $\Delta 6$  apoA-I signal peptide-minus apolipoproteins would not be translocated into the ER but instead would directly enter the quality control pathway,



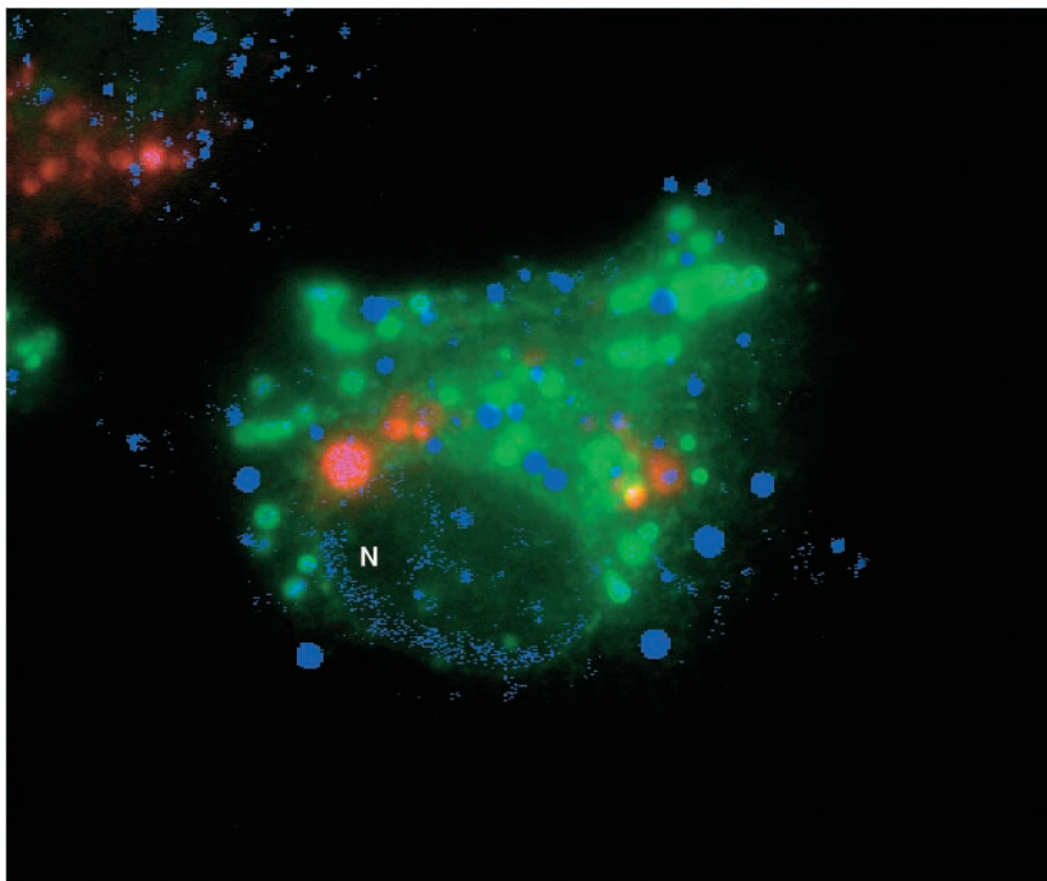


**Fig. 8.** Coimmunolocalization of lysosomes and cytoplasmic inclusions in COS-1 cells transfected with  $\Delta 6$  apoA-I. Transiently transfected COS-1 cells were double labeled, as described in Materials and Methods, to establish whether  $\Delta 6$  apoA-I cytoplasmic inclusions labeled with fluorescein colocalize with the organelle-specific lysosomal marker, cathepsin D, labeled with rhodamine. In this single cell image, the composite or colocalization of  $\Delta 6$  apoA-I (green) and lysosomes (red) appears yellow, indicating that the majority of the bagels, or cytoplasmic inclusions, are not coincident with lysosomes. Classic lipid droplets were also visualized using osmium-thiocarbohydrazide-osmium and are colored blue. N, nucleus.

where wild-type apoA-I would be degraded and  $\Delta 6$  apoA-I would associate with lipid-forming cytosolic inclusions. Results from these studies showed that both wild-type and  $\Delta 6$  apoA-I signal peptide-minus proteins accumulated as dense, irregularly shaped, brightly fluorescent structures, similar to those seen in the apoA-I-overexpressing COS-1 cells (Fig. 7E–H). Pulse-chase studies in COS-1 cells transfected with signal peptide-minus wild-type and  $\Delta 6$  apoA-I yielded only partially degraded or truncated forms of labeled apoA-I. No “full-length” wild-type or  $\Delta 6$  apoA-I was present in the cell pellet or medium (data not shown). These results suggest that once the apolipoproteins were directed from the ER they rapidly entered the quality control pathway and were degraded, with no evidence of accumulation in the cytoplasm to form discrete lipid:apolipoprotein inclusions.

Another entry point into the quality control pathway would be the targeting of  $\Delta 6$  apoA-I to the lysosomes. To investigate this possibility, double-label immunofluorescence microscopy was used to determine if the  $\Delta 6$  apoA-I bagel structures colocalized with the lysosome-specific

marker cathepsin D. In these studies, COS-1 cells were transfected with  $\Delta 6$  apoA-I cDNA. As shown in **Fig. 8**, immunofluorescence staining for  $\Delta 6$  apoA-I-transfected COS-1 cells showed uniformly shaped cytoplasmic inclusions or bagels (green) that did not appear to overlay the staining of lysosomes (red) or the classic neutral lipid droplets (blue).

## DISCUSSION

In these studies, we demonstrate by both biochemical and microscopic techniques that newly synthesized  $\Delta 6$  apoA-I accumulates within the cell cytoplasm as lipid:protein inclusions. Of the apoA-I mutants tested, only the production of  $\Delta 6$  apoA-I consistently showed the formation of cytoplasmic bagel inclusions, with minor ER/Golgi localization. Other apoA-I helix deletion and/or substitution mutants possessing low secretory properties showed apoA-I localization predominantly in the ER/Golgi, with virtually no cytoplasmic bagels. These data suggest that de-

letion of helix 6 renders an unstable conformation leading to protein aggregation and the formation of discrete lipid:protein structures whose physiological implications are unknown.

The synthesis, folding, and intracellular trafficking of apoA-I, as with all proteins, is carefully monitored by the quality control system (49). Like other misfolded proteins, mutant apoA-I is probably retained in the ER and exposed to ER resident chaperones in an attempt to fold the protein correctly (50). Here, a misfolded protein may aggregate and undergo retrograde translocation into the cytosol followed by ubiquitination and proteasomal degradation (51, 52). Once the misfolded protein enters the cytoplasm, a number of quality control mechanisms are directed at preventing aggregation and the formation of inclusion bodies that if not controlled could disrupt cellular functions. Usually, the capacity of the proteasome is not exceeded by the rate of retrograde translocation (50, 53–55). Hence, for most misfolded protein substrates, it is rare to observe extensive accumulation of the misfolded protein within the cytosol. In some instances of protein overexpression and/or pharmacologic inhibition of proteasomal function, misfolded proteins can accumulate within the cytosol. In the most well-characterized example, specific mutants of the cystic fibrosis transmembrane conductance regulator form microtubule-dependent inclusion bodies known as aggresomes. These entities have characteristic compositional properties that, in addition to the misfolded protein, include cytoplasmic chaperones and components of the proteasome. Typically, aggresomes appear to be wrapped in cage-like structures formed by intermediate filament proteins, such as vimentin, and generally migrate to and accumulate at microtubule-organizing centers (54, 55).

In the case of  $\Delta 6$  apoA-I, a novel form of cytoplasmic inclusions has been observed resulting from misfolding and retrograde translocation. These studies suggest that after retrograde translocation, misfolded  $\Delta 6$  apoA-I rapidly associates with phospholipid, forming bagel-shaped structures or inclusion bodies in both lipoprotein- and non-lipoprotein-producing cells. Because more than 60% of newly synthesized apoA-I is thought to be secreted from hepatocytes in a lipid-free form (17, 18), the phospholipid recruited into the  $\Delta 6$  apoA-I inclusions is likely derived from intracellular membranes. These structures appear to stabilize the conformation of apoA-I against proteasomal or other forms of intracellular degradation. Thus, the accumulation of the lipid:apolipoprotein bagels suggests that these complexes are extremely resistant to proteasomal degradation and may be further stabilized by fusing together to form even larger structures, as suggested by the brefeldin A studies.


Unexpectedly, the apoA-I mutants  $\Delta 7$ , L159R, and A154P apoA-I did not accumulate in the cytoplasm or form bagel structures, although they all had poor secretion efficiencies. These results suggest that the structural alterations induced by these helix 6 and 7 mutations do not cause the same degree of protein aggregation and/or that these mutant proteins are degraded by the protea-

some before they can form inclusion bodies. Taken together, these data suggest that apoA-I helix 6 plays a key role in native protein folding. In the absence of this amphipathic helix, the apolipoprotein is poorly soluble, forming a precipitate. Perhaps the poor solubility is attributable to an inability of the apolipoprotein to stabilize its hydrophobic N- and C-terminal ends in the absence of helix 6.

Physiologically, the implications of poor apoA-I secretion efficiency and inclusion body formation are unknown. Studies of the apoA-I helix 6 deletion mutation showed that Tg  $\Delta 6$  apoA-I mice expressing the  $\Delta 6$  apoA-I mutant protein and carrying one mouse allele (Tg  $\Delta 6$  +/–) reported low plasma HDL levels, with the  $\Delta 6$  apoA-I fractional catabolic rate  $\sim 1.7$ -fold greater than that for wild-type apoA-I (25). However, these mice also showed a 35% lower production rate for the  $\Delta 6$  apoA-I protein, with no apparent decrease in wild-type apoA-I production compared with control mice (25). These findings led us to ask the question: was retained  $\Delta 6$  apoA-I rapidly degraded within the cell, and would the production and/or secretion of  $\Delta 6$  apoA-I “negatively” influence the secretion of wild-type apoA-I and contribute to a “dominant-negative phenotype”?

Only a few apoA-I mutations display a dominant-negative phenotype, defined as the dominant effect of one mutant allele on the normal allele in heterozygous carriers (23). These mutations are predominantly in helices 6 and 7. Because the  $\Delta 6$  apoA-I mutant lacks the complete proline-punctuated repeat of helix 6 (143–164) in native apoA-I, it is similar to apoA-I Seattle E146 $\Delta$ R160 (56) described in humans. The mutant apoA-I Seattle was characterized in an individual with less than 10% of normal HDL apoA-I concentrations, despite the presence of one normal apoA-I allele. In the Tg  $\Delta 6$  apoA-I mouse studies, it was concluded that the dominant-negative influence could be explained, in part, by the competitive inhibition of  $\Delta 6$  apoA-I over normal mouse apoA-I in the activation of LCAT, thus accounting for the increase in fractional catabolic rate (24, 25) and the low concentration of HDL in plasma. However, contributing to the phenotype, the production rate of  $\Delta 6$  apoA-I was 20–25% lower than that for wild-type apoA-I, suggesting that the  $\Delta 6$  apoA-I concentrations in plasma may also be a product of low secretion and assembly of nascent HDL as well as of rapid catabolism of the cholesteryl ester-poor HDL particles. A second mutation showing the dominant-negative phenotype is apoA-I Fin or L159R apoA-I. Adenovirus-infected apoA-I<sup>–/–</sup> mice showed that L159R apoA-I, first described in heterozygous humans (43, 44), was associated with very low levels of HDL in plasma. The HDL present in these mice was severely underlipidated with cholesteryl ester. Adenovirus overexpression of L159R apoA-I in apoA-I<sup>–/–</sup> mice was also associated with enhanced degradation of the mutant protein in plasma (26). Whether degradation of the mutant apoA-I in plasma was the cause of its underlipidation or a result of its underlipidation was not clear; however, mouse primary hepatocytes infected with apoA-I Fin adenovirus secreted 30% less L159R apoA-I than did wild-type apoA-I adenovirus-infected livers.

Recently, investigators have shown that primary mouse hepatocytes from mice homozygous for a targeted substitution of apoA-I Milano or R173C apoA-I for wild-type mouse apoA-I had a 42% reduction in hepatic secretion of the mutant protein (27). This dominant-negative mutation has been extensively studied in humans and in animal models. The cysteine residue has been shown to form homodimers and heterodimers in plasma, and the presence of this mutation has been associated with "protection against coronary heart disease" (57, 58). The "knock in" mice also showed the characteristic underlipidated or cholesteryl ester-poor plasma HDL. However, in this model, a dominant effect of the mutant protein over the wild-type human protein was not observed. Mice heterozygous for human apoA-I Milano and human wild-type apoA-I showed plasma levels similar to those of mice expressing only human wild-type apoA-I. Primary mouse hepatocytes heterozygous for apoA-I Milano had depressed apoA-I Milano secretion, similar to that of homozygous cells, suggesting that the dominant-negative phenotype was not at the level of protein processing and secretion.

In summary, these studies show that the apoA-I 143–164 residue domain corresponding to helix 6 is absolutely required for proper folding of the protein and its efficient secretion from cells. The unique bagel-like inclusions composed of phospholipid and misfolded or aggregated  $\Delta 6$  apoA-I appear to result from the transport of  $\Delta 6$  apoA-I from the ER to the cytosol, where the apolipoprotein binds to phospholipid and the inclusions become resistant to the intracellular degradation machinery. The overall consequence of bagel formation does not appear to have any impact on the production or secretion of human wild-type apoA-I and thus only appears to contribute to the dominant-negative phenotype by reducing the overall apolipoprotein production. Therefore, we conclude that apoA-I helix 6 plays an essential role in directing the proper folding of native apoA-I and that without this essential domain the mutant protein forms unique aggregated lipid:apolipoprotein structures that accumulate in the cell cytoplasm. 

The authors thank John Mayben, Nell Nordin, and Mary Kearns for their technical assistance during the course of these studies. These studies were supported by Public Health Service grants from the National Institutes of Health (HL-49373 and HL-64163; M.G.S.T.).

## REFERENCES

- Higuchi, K., S. W. Law, J. M. Hoeg, U. K. Schumacher, N. Meglin, and H. B. Brewer, Jr. 1988. Tissue-specific expression of apolipoprotein A-I (ApoA-I) is regulated by the 5'-flanking region of the human apoA-I gene. *J. Biol. Chem.* **263**: 18530–18536.
- Glomset, J. A. 1968. The plasma lecithin:cholesterol acyltransferase reaction. *J. Lipid Res.* **9**: 155–167.
- Fielding, C. J., and P. E. Fielding. 1995. Molecular physiology of reverse cholesterol transport. *J. Lipid Res.* **36**: 211–228.
- Rigotti, A., H. E. Miettinen, and M. Krieger. 2003. The role of the high-density lipoprotein receptor SR-BI in the lipid metabolism of endocrine and other tissues. *Endocr. Rev.* **24**: 357–387.
- Schaefer, E. J. 1994. Familial lipoprotein disorders and premature coronary artery disease. *Med. Clin. North Am.* **78**: 21–39.
- Castelli, W. P., R. J. Garrison, P. W. F. Wilson, and S. Abbott. 1986. Incidence of coronary heart disease and lipoprotein cholesterol levels: the Framingham Study. *J. Am. Med. Assoc.* **156**: 2835–2838.
- Hamilton, R. L., M. C. Williams, C. J. Fielding, and R. J. Havel. 1976. Discoidal bilayer structure of nascent high density lipoproteins from perfused rat liver. *J. Clin. Invest.* **58**: 667–680.
- Eisenberg, S. 1984. High density lipoprotein metabolism. *J. Lipid Res.* **25**: 1017–1058.
- Hamilton, R. L., A. Moorehouse, and R. J. Havel. 1991. Isolation and properties of nascent lipoproteins from highly purified rat hepatocytic Golgi fractions. *J. Lipid Res.* **32**: 529–543.
- Rusinol, A., H. Verkade, and J. E. Vance. 1993. Assembly of rat hepatic very low density lipoproteins in the endoplasmic reticulum. *J. Biol. Chem.* **268**: 3555–3562.
- Banerjee, D., and C. M. Redman. 1983. Biosynthesis of high density lipoprotein by chicken liver: nature of nascent intracellular high density lipoprotein. *J. Cell Biol.* **96**: 651–660.
- LeCureux, L. W., F. J. Kezdy, and B. W. Wattenberg. 1994. The efficiency and kinetics of secretion of apolipoprotein A-I in hepatic and non-hepatic cells. *Atherosclerosis.* **106**: 225–233.
- Banerjee, D., T. K. Mukherjee, and C. M. Redman. 1985. Biosynthesis of high density lipoprotein by chicken liver: intracellular transport and proteolytic processing of nascent apolipoprotein A-I. *J. Cell Biol.* **101**: 1219–1226.
- Dixon, J. L., R. Battini, S. Ferrari, C. M. Redman, and D. Banerjee. 1989. Expression and secretion of chicken apolipoprotein AI in transfected COS cells. *Biochim. Biophys. Acta.* **1009**: 47–53.
- Dixon, J. L., R. Chattapadhyay, T. R. Huima, C. M. Redman, and D. Banerjee. 1992. Biosynthesis of lipoprotein: location of nascent apoA-I and apoB in the rough endoplasmic reticulum of chicken hepatocytes. *J. Cell Biol.* **117**: 1161–1169.
- Howell, K. E., and G. E. Palade. 1982. Heterogeneity of lipoprotein particles in hepatic Golgi fractions. *J. Cell Biol.* **92**: 833–845.
- Chisholm, J. W., E. R. Burlinson, G. S. Shelness, and J. S. Parks. 2002. ApoA-I secretion from HepG2 cells: evidence for the secretion of both lipid-poor apoA-I and intracellularly assembled nascent HDL. *J. Lipid Res.* **43**: 36–44.
- Kiss, R. S., D. C. McManus, V. Franklin, W. L. Tan, A. McKenzie, G. Chimini, and Y. L. Marcel. 2003. The lipidation by hepatocytes of human apolipoprotein A-I occurs by both ABCA1-dependent and -independent pathways. *J. Biol. Chem.* **278**: 10119–10127.
- Marcel, Y. L., and R. S. Kiss. 2003. Structure-function relationships of apolipoprotein A-I: a flexible protein with dynamic lipid associations. *Curr. Opin. Lipidol.* **14**: 151–157.
- Klon, A. E., J. P. Segrest, and S. C. Harvey. 2002. Comparative models for human apolipoprotein A-I bound to lipid in discoidal high-density lipoprotein particles. *Biochemistry.* **41**: 10895–10905.
- Brouillette, C. G., G. M. Anantharamaiah, J. A. Engler, and D. W. Borhani. 2001. Structural models of human apolipoprotein A-I: a critical analysis and review. *Biochim. Biophys. Acta.* **1531**: 4–46.
- Klon, A. E., M. K. Jones, J. P. Segrest, and S. C. Harvey. 2000. Molecular belt models for the apolipoprotein A-I Paris and Milano mutations. *Biophys. J.* **79**: 1679–1685.
- Sorci-Thomas, M. G., and M. J. Thomas. 2002. The effects of altered apolipoprotein A-I structure on plasma HDL concentration. *Trends Cardiovasc. Med.* **12**: 121–128.
- Sorci-Thomas, M. G., M. Thomas, L. Curtiss, and M. Landrum. 2000. Single repeat deletion in apoA-I blocks cholesterol esterification and results in rapid catabolism of D6 and wild-type apoA-I in transgenic mice. *J. Biol. Chem.* **275**: 12156–12163.
- Baralle, M., and F. E. Baralle. 2000. Genetics and molecular biology. *Curr. Opin. Lipidol.* **11**: 653–656.
- McManus, D. C., B. R. Scott, V. Franklin, D. L. Sparks, and Y. L. Marcel. 2001. Proteolytic degradation and impaired secretion of an apolipoprotein A-I mutant associated with dominantly inherited hypoalphalipoproteinemia. *J. Biol. Chem.* **276**: 21292–21302.
- Parolini, C., G. Chiesa, Y. Zhu, T. Forte, S. Caligari, E. Gianazza, M. G. Sacco, C. R. Sirtori, and E. M. Rubin. 2003. Targeted replacement of mouse apolipoprotein A-I with human ApoA-I or the mutant ApoA-IMilano. Evidence of APOA-IM impaired hepatic secretion. *J. Biol. Chem.* **278**: 4740–4746.
- Sorci-Thomas, M. G., J. S. Parks, M. W. Kearns, G. N. Pate, C. Zhang, and M. J. Thomas. 1996. High level secretion of wild-type



- and mutant forms of human proapoA-I using baculovirus-mediated Sf-9 cell expression. *J. Lipid Res.* **37**: 673–683.
29. Sorci-Thomas, M., M. W. Kearns, and J. P. Lee. 1993. Apolipoprotein A-I domains involved in lecithin-cholesterol acyltransferase activation. Structure: function relationships. *J. Biol. Chem.* **268**: 21403–21409.
  30. Li, H. H., M. J. Thomas, W. Pan, E. Alexander, M. Samuel, and M. G. Sorci-Thomas. 2001. Preparation and incorporation of probe-labeled apoA-I for fluorescence resonance energy transfer studies of rHDL. *J. Lipid Res.* **42**: 2084–2091.
  31. Sorci-Thomas, M. G., L. Curtiss, J. S. Parks, M. J. Thomas, and M. W. Kearns. 1997. Alteration in apolipoprotein A-I 22-mer repeat order results in a decrease in lecithin:cholesterol acyltransferase reactivity. *J. Biol. Chem.* **272**: 7278–7284.
  32. Sorci-Thomas, M. G., L. Curtiss, J. S. Parks, M. J. Thomas, M. W. Kearns, and M. Landrum. 1998. The hydrophobic face orientation of apolipoprotein A-I amphipathic helix domain 143–164 regulates lecithin:cholesterol acyltransferase activation. *J. Biol. Chem.* **273**: 11776–11782.
  33. Ingram, M. F., and G. S. Shelness. 1997. Folding of the amino-terminal domain of apolipoprotein B initiates microsomal triglyceride transfer protein-dependent lipid transfer to nascent very low density lipoprotein. *J. Biol. Chem.* **272**: 10279–10286.
  34. Shelness, G. S., K. C. Morris-Rogers, and M. F. Ingram. 1994. Apolipoprotein B48-membrane interactions. Absence of transmembrane localization to nonhepatic cells. *J. Biol. Chem.* **269**: 9310–9318.
  35. Colvin, P., E. Moriguchi, H. Barrett, J. Parks, and L. Rudel. 1998. Production rate determines plasma concentration of large high density lipoprotein in non-human primates. *J. Lipid Res.* **39**: 2076–2085.
  36. Koritnik, D. L., and L. L. Rudel. 1983. Measurement of apolipoprotein A-I concentration in nonhuman primate serum by enzyme-linked immunosorbent assay (ELISA). *J. Lipid Res.* **24**: 1639–1645.
  37. Fiske, C. A., and Y. SubbaRow. 1925. The colorimetric determination of phosphorus. *J. Biol. Chem.* **66**: 375–400.
  38. Willingham, M. C., and I. Pastan. 1985. Immunofluorescence techniques. In *An Atlas of Immunofluorescence in Cultured Cells*. I. Pastan, and Mark C. Willingham, editors. Academic Press, Orlando, FL. 1–13.
  39. Willingham, M. C., and I. Pastan. 1985. Morphologic methods in the study of endocytosis in cultured cells. In *Endocytosis*. I. Pastan and M. C. Willingham, editors. Plenum Publishing, New York. 281–321.
  40. Willingham, M. C., and A. V. Rutherford. 1984. The use of the osmium-thiocarbonyl osmium (OTO) and ferrocyanide-reduced osmium methods to enhance membrane contrast and preservation in cultured cells. *J. Histochem. Cytochem.* **32**: 455–460.
  41. Zannis, V. I., S. K. Karathanasis, H. T. Keutmann, G. Goldberger, and J. L. Breslow. 1983. Intracellular and extracellular processing of human apolipoprotein A-I: isoprotein 2 is a propeptide. *Proc. Natl. Acad. Sci. USA.* **80**: 2574–2578.
  42. Banerjee, D., G. Grienering, J. L. Parkes, T. Kumar, T. K. Mukherjee, and C. M. Redman. 1986. Regulation of apo-A-I processing in cultured hepatocytes. *J. Biol. Chem.* **261**: 9844–9849.
  43. Miettinen, H. E., M. Jauhiainen, H. Gylling, S. Ehnholm, A. Palomaki, T. A. Miettinen, and K. Kontula. 1997. Apolipoprotein A-I<sub>FIN</sub> (Leu159→Arg) mutation affects lecithin-cholesterol acyltransferase activation and subclass distribution of HDL but not cholesterol efflux from fibroblasts. *Arterioscler. Thromb. Vasc. Biol.* **17**: 3021–3032.
  44. Miettinen, H. E., H. Gylling, T. A. Miettinen, J. Viikari, L. Paulin, and K. Kontula. 1997. Apolipoprotein A-I<sub>FIN</sub>. Dominantly inherited hypoalphalipoproteinemia due to a single base substitution in the apolipoprotein A-I gene. *Arterioscler. Thromb. Vasc. Biol.* **17**: 83–90.
  45. Johnston, J. A., C. L. Ward, and R. R. Kopito. 1998. Aggresomes: a cellular response to misfolded proteins. *J. Cell Biol.* **143**: 1883–1898.
  46. Garcia-Mata, R., Y. S. Gao, and E. Sztul. 2002. Hassles with taking out the garbage: aggravating aggresomes. *Traffic.* **3**: 388–396.
  47. Buckig, A., R. Tikkanen, V. Herzog, and A. Schmitz. 2002. Cytosolic and nuclear aggregation of the amyloid beta-peptide following its expression in the endoplasmic reticulum. *Histochem. Cell Biol.* **118**: 353–360.
  48. Wu, Y., I. Whitman, E. Molmenti, K. Moore, P. Hippenmeyer, and D. H. Perlmutter. 1994. A lag in intracellular degradation of mutant alpha 1-antitrypsin correlates with the liver disease phenotype in homozygous PiZZ alpha 1-antitrypsin deficiency. *Proc. Natl. Acad. Sci. USA.* **91**: 9014–9018.
  49. Elgaard, L., M. Molinari, and A. Helenius. 1999. Setting the standards: quality control in the secretory pathway. *Science.* **286**: 1882–1888.
  50. Kopito, R. R. 1999. Biosynthesis and degradation of CFTR. *Physiol. Rev.* **79**: 167–173.
  51. Hurlley, S. M., and A. Helenius. 1989. Protein oligomerization in the endoplasmic reticulum. *Annu. Rev. Cell Biol.* **5**: 277–307.
  52. Klausner, R. D., and R. Sitia. 1990. Protein degradation in the endoplasmic reticulum. *Cell.* **62**: 611–614.
  53. Wickner, S., M. R. Maurizi, and S. Gottesman. 1999. Posttranslational quality control: folding, refolding, and degrading proteins. *Science.* **286**: 1888–1893.
  54. Kopito, R. R. 2000. Aggresomes, inclusion bodies and protein aggregation. *Trends Cell Biol.* **10**: 524–530.
  55. Trombetta, E. S., and A. J. Parodi. 2003. Quality control and protein folding in the secretory pathway. *Annu. Rev. Cell Dev. Biol.* **19**: 649–676.
  56. Deeb, S. S., M. C. Cheung, R. Peng, A. C. Wolf, R. Stern, J. J. Albers, and R. H. Knopp. 1991. A mutation in the human apolipoprotein A-I gene. Dominant effect on the level and characteristics of plasma high density lipoproteins. *J. Biol. Chem.* **266**: 13654–13660.
  57. Weisgraber, K. H., T. P. Bersot, R. W. Mahley, G. Franceschini, and C. R. Sirtori. 1980. A-I<sub>Milano</sub> apoprotein. Isolation and characterization of a cysteine-containing variant of the A-I apoprotein from human high density lipoproteins. *J. Clin. Invest.* **66**: 901–907.
  58. Sirtori, C. R., L. Calabresi, G. Franceschini, D. Baldassarre, M. Amato, J. Johansson, M. Salvetti, C. Monteduro, R. Zulli, M. L. Muiesan, and E. Agabiti-Rosei. 2001. Cardiovascular status of carriers of the apolipoprotein A-I<sub>Milano</sub> mutant—the Limone sul Garda Study. *Circulation.* **103**: 1949–1954.